Dalton Transactions

Accepted Manuscript

ROYAL SOCIETY OF CHEMISTRY

www.rsc.org/dalton

Cite this: DOI: 10.1039/c0xx00000x

www.rsc.org/xxxxxx

ARTICLE TYPE

Band gap-tunable potassium doped graphitic carbon nitride with enhanced mineralization ability

Shaozheng Hu, [a,*] Fayun Li, [a] Zhiping Fan, [a] Fei Wang, [b] Yanfeng Zhao [b] and Zhenbo Lv [c,*]

Received (in XXX, XXX) Xth XXXXXXXXX 20XX, Accepted Xth XXXXXXXXX 20XX

DOI: 10.1039/b000000x

A band gap-tunable potassium doped graphitic carbon nitride with enhanced mineralization ability was prepared using dicyandiamide monomer and potassium hydrate as precursor. X-ray diffraction (XRD), N_2 adsorption, UV-Vis spectroscopy, Fourier transform infrared spectra (FT-IR), Scanning electron microscopy (SEM), Photoluminescence (PL) and X-ray photoelectron spectroscopy (XPS) were used to characterize the prepared catalysts. The CB and VB potentials of graphitic carbon nitride could be tuned from -1.09 and +1.56 eV to -0.31 and +2.21 eV by controlling the K concentration. Besides, the addition of potassium inhibited the crystal growth of graphitic carbon nitride, enhanced the surface area and increased the separation rate of photogenerated electrons and holes. The visible-light-driven Rhodamine B (RhB) photodegradation and mineralization performances were significantly improved after potassium doping. The possible influence mechanism of potassium concentration on photocatalytic performance was proposed.

Introduction

Nowadays, due to the significant energy and environmental crises, looking for new energy resources and strategies for pollution degradation become much more important. With outstanding virtues, including non-pollution and inexhaustible supply, solar energy is considered as one of the most promising candidate to resolve these problems. However, the low efficiency of the energy conversion still restricts its practical application. Recently, a metal-free visible-light photocatalyst graphitic carbon nitride (g-C_3N_4) has attracted intensive interest for its promising applications in splitting water to produce H_2,[1] decomposition of organic pollutants[2] and organic synthesis.[3] That attributes to the moderate band gap (2.7 eV), high chemical and thermal stability and fascinating electronic property of g-C_3N_4. However, the rapid photogenerated electron-hole pair recombination leads to the low activity in practical applications.[4,5]

Development of g-C_3N_4 based heterostructured photocatalysts is one of the effective strategies to solve the problem. Because heterojunctions are responsible for an efficient photogenerated charge interface migration, it is crucial for increasing the activity of photocatalysts. It is known that the energy level matching of two semiconductors is significant to form the heterojunction. A tunable band structure of g-C_3N_4 is convenient to match the energy level with other semiconductor, thus is beneficial for the forming of the heterojunction. In general, band gaps of semiconductor nanocrystals may be controlled by the grain size, which called quantum size effect.[6] This size-dependent band gap of quantum dots has been extensively studied. However, the preparation of quantum dots often requires harsh conditions and complicated preparation procedure. Another facile and flexible approach is doping.[7-13] Orbital hybridization occurs between dopant orbital and molecular orbital of g-C_3N_4, leading to the tunable electronic structure and potential of VB and CB.

Because of the active chemical properties, alkali metals are widely used in the catalytic reaction.[14-17] Salinas et al. prepared potassium-supported TiO_2 catalysts for transesterification reaction.[14] Chu et al. prepared halogen-free K^+-modified CuO_x/SBA-15 for propylene epoxidation by molecular oxygen.[15] They suggested that Cu(I) on the surface modified by K^+ was responsible for the epoxidation. Pekridis et al. reported the modification effect of K^+ on N_2O reduction by alkanes over Pd/γ-Al_2O_3 catalysts.[16] Qu et al. reported the effects of alkali metal on the toluene catalytic oxidation over the manganese oxide supported on SBA-15.[17] They found that the catalysts, with K/Mn in the range of 0.15/1~0.18/1, exhibited better performances in the catalytic oxidation of toluene. However, little attention has been given to the investigation of the influence of alkali metal on the promotion of photocatalytic activity.[18,19] Grzechulska et al.[18] added a series of alkali to crystallized TiO_2 slurry to prepare alkali metal modified TiO_2 catalysts. The result of photocatalytic decomposition of oil indicated that the activity followed the order: TiO_2/KOH > TiO_2/$Ca(OH)_2$ > TiO_2/$Ba(OH)_2$ > TiO_2 (anatase). Chen et al. prepared K^+-doped TiO_2 by the sol-gel method and thermal treatment.[19] Calcination leads to the formation of $K_{4-4x}Ti_xO_2$, which x value corresponds to promoters of photoactivity. K^+ doping reduced recombination of the e^- and h^+ pair, enhanced the interfacial charge transfer, and improved reactants adsorption on the catalyst. Besides, the appropriate K^+ concentration could reduce crystal size, increase surface area and raise the crystal transition temperature.

In addition to superior catalytic performance, the

mineralization ability in the degradation process is a key issue impeded the practical application of photocatalysts. The photocatalytic degradation of organic compound is a complex process, and many intermediate products are produced, especially when the initial substrate is complicated. Many intermediate products are more harmful to human health than the initial pollutant, thus thorough decomposition of the pollutant is necessary. In this work, a band gap-tunable potassium doped graphitic carbon nitride with enhanced mineralization ability was prepared for the first time using dicyandiamide monomer and potassium hydrate as precursor. The photocatalytic activity and stability were evaluated in the photocatalytic degradation of RhB under visible light. The effects of doping on the structural property, optical property and photocatalytic performance of as-prepared catalysts were discussed in detail.

Experimental

Preparation and characterization

In a typical experiment, 2 g dicyandiamide was dispersed into 10 ml deionized water under stirring. Then 10 ml KOH solution (0.02, 0.05, 0.07 and 0.09 M) was added. The obtained suspension was heated to 100 ^{o}C to remove the water. The solid product was dried at 80 ^{o}C in oven, followed by milling and annealing at 520 ^{o}C for 2 h (at a rate of 5 ^{o}C·min^{-1}). The obtained product was denoted as K(x)-CN, where x corresponds to the KOH concentration. When 10 ml deionized water or 10 ml NH_4OH (0.05 M) was used to replace 10 ml KOH (0.05 M), following the same procedure as the synthesis of K(0.05)-CN, two products of g-C_3N_4 and OH(0.05)-CN can be obtained. For comparison, as-prepared g-C_3N_4 was dispersed into 10 ml KOH (0.05 M). The obtained suspension was stirred for 10 h, and heated to 100 ^{o}C to remove the water. The solid product was dried and denoted as g-C_3N_4/KOH.

XRD patterns of the prepared samples were recorded on a Rigaku D/max-2400 instrument using Cu-Kα radiation (λ = 1.54 Å). The scan rate, step size, voltage and current was 0.05 ^{o}/min, 0.01 ^{o}, 40kV and 30 mA, respectively. UV-vis spectroscopy measurement was carried out on a JASCO V-550 model UV-vis spectrophotometer, using $BaSO_4$ as the reflectance sample. Fourier transform infrared spectra (FT-IR) were obtained on a Nicolet 20DXB FT-IR spectrometer. Nitrogen adsorption was measured at -196 °C on a Micromeritics 2010 analyzer. All the samples were outgassed at 393K for 3 h before the measurement. BET surface area (S_{BET}) was calculated according to the adsorption isotherm. The morphology of prepared catalyst was observed by using a scanning electron microscope (SEM, JSM 5600LV, JEOL Ltd.). ICP was performed to determine the actual K concentration on a Perkin-Elmer Optima 3300DV apparatus. XPS measurements were conducted on a Thermo Escalab 250 XPS system with Al Kα radiation as the exciting source. Curve fits were made using CasaXPS, while the relative sensitivity factors and asymmetry functions were taken from the PHI ESCA handbook. The binding energies were calibrated by referencing the C 1s peak (284.6 eV) to reduce the sample charge effect. Photoluminescence (PL) spectra were measured at room temperature with a fluorospectrophotometer (FP-6300), using Xe lamp as excitation source.

Photocatalytic Reaction

RhB was selected as the model compound to evaluate the photocatalytic performance of the prepared g-C_3N_4 based catalysts in an aqueous solution under visible light irradiation. In 200 ml aqueous solution of RhB (10 ppm), 0.05 g catalyst was dispersed and the solution was left in an ultrasound generator for 10 min. The suspension was transferred into a self-designed glass reactor, stirred for 30 min in darkness to achieve the adsorption equilibrium. In the photoreaction , the suspension was exposed to a 250 W high-pressure sodium lamp with main emission in the range of 400-800 nm and air was bubbled at 130 ml/min through the solution. The UV light portion of sodium lamp was filtered by 0.5 M $NaNO_2$ solution.[20] All runs were conducted at ambient pressure at 30 °C. At given time intervals, 4 ml suspension was taken and immediately centrifuged to separate the liquid phase from the solid catalyst. The concentrations of RhB before and after reaction were measured by UV-Vis spectrophotometer at wavelength of 550 nm.

Results and discussion

Fig. 1 shows the XRD patterns of as-prepared g-C_3N_4 and K(x)-CN. The patterns of g-C_3N_4 and K(x)-CN exhibit two peaks at 13.1^{o} and 27.3^{o}, corresponding to (100) and (002) crystal planes of g-C_3N_4 (JCPDS 87-1526).[21] These two peaks show gradually decreased intensity with increasing the potassium concentration, which suggests that the crystal growth of graphitic carbon nitride inhibited by introduction of potassium. No peak for potassium related species is observed in the pattern of K(x)-CN. Whereas, the obvious shifts toward a lower 2θ value are observed for all the K(x)-CN catalysts. This is probably because potassium doped into interstitial sites of in-planar g-C_3N_4, which enlarged the interlayer spacing. In Fig. S1, no peak shift in the pattern of g-C_3N_4/KOH and OH(0.05)-CN is shown by comparing with g-C_3N_4. This hints two kinds of information. First of all, the existence form of potassium species in g-C_3N_4/KOH and K(0.05)-CN is different. Secondly, such lattice distortion shown in Fig. 1 is not caused by the alkalization treatment but by potassium doping.

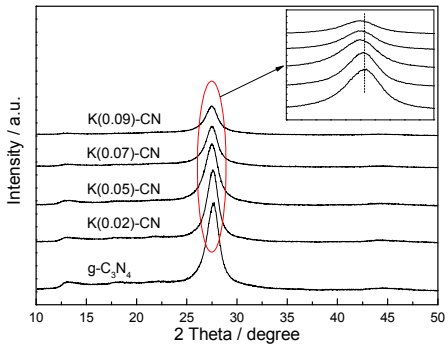

Fig. 1 XRD patterns of as-prepared g-C_3N_4 and K(x)-CN.

FT-IR spectra of as-prepared g-C_3N_4 based catalysts (Fig. S2) show that the peak at 1640 cm^{-1} is attributed to C-N stretching vibration modes and the peaks in the range of 1200~1400 cm^{-1} is for the stretching of aromatic C-N. The bands near 800 and 3200

cm^{-1} attribute to out-of-plane bending modes of C-N heterocycles and stretching vibration of N-H bond, associating with uncondensed aminogroups.[22] For K(x)-CN, all the characteristic vibrational peaks of g-C_3N_4 are observed. The vibrations of K-related group are not observed, suggesting that the framework of g-C_3N_4 is not changed after doping.

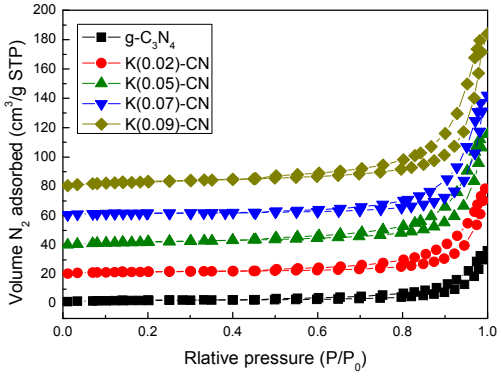

Fig. 2 N_2 adsorption-desorption isotherms of g-C_3N_4 and K(0.05)-CN.

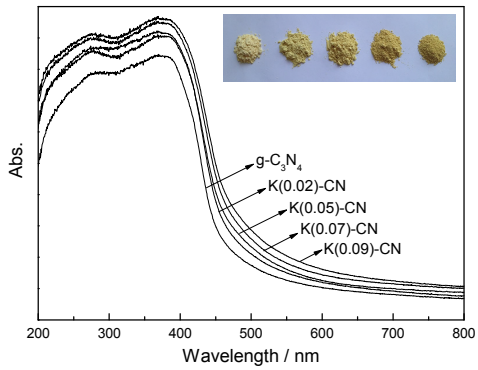

Fig. 3 UV-Vis diffuse reflectance spectra of as-prepared g-C_3N_4 based catalysts.

Nitrogen adsorption and desorption isotherms were measured to characterize the specific surface area of as-prepared g-C_3N_4 based catalysts (Fig. 2). Both g-C_3N_4 and K(x)-CN show a type IV isotherm with H3 hysteresis loop, suggesting the presence of mesopores. The hysteresis loop in the low pressure range ($0.4<P/P_0<0.9$) is associated with the intra-aggregated pores. The high-pressure hysteresis loop ($0.9<P/P_0<1$) is related to the larger pores formed between secondary particles. The BET specific surface areas (S_{BET}) of g-C_3N_4, K(0.02)-CN, K(0.05)-CN, K(0.07)-CN and K(0.09)-CN are calculated to be 8.9, 18.8, 26.9, 29.2 and 30.8 $m^2 \cdot g^{-1}$, respectively. This increased S_{BET} is probably due to potassium doping inhibited the crystal growth of graphitic carbon nitride, leading to the formation of more secondary particles. Such large S_{BET} is favorable to the photocatalytic performance because it can promote adsorption, desorption and diffusion of reactants and products.[23]

The optical absorption of as-prepared g-C_3N_4 based catalysts were measured using UV-Vis diffuse reflectance spectra. The band gaps are estimated from the tangent lines in the plots of the square root of the Kubelka-Munk functions against the photon energy (Fig. S3).[24] As presented in Fig. 3, the main absorption edge of g-C_3N_4 occurs at ca. 460 nm. The band gap for g-C_3N_4 is about 2.65 eV, which is in good agreement with the value reported in previous literature.[25] In the case of K(x)-CN, the obvious red shifts of the absorption band are observed. However, no obvious difference among g-C_3N_4, g-C_3N_4/KOH and OH(0.05)-CN is shown in Fig. S4. This hints two kinds of information. First of all, the existence form of potassium species in g-C_3N_4/KOH and K(x)-CN is different, which is consistent with XRD pattern. Secondly, such shift of absorption band is not caused by the alkalization treatment but by potassium doping. The inset in Fig. 3 reveals that pure g-C_3N_4 is light yellow in color. The color of K(x)-CN gradually deepens with increasing the potassium concentration. The band gap energy decreases to 2.6, 2.57, 2.55 and 2.52 eV for K(0.02)-CN, K(0.05)-CN, K(0.07)-CN and K(0.09)-CN, respectively. This indicates that potassium concentration has a strong influence on the optical property and band structure of as-prepared g-C_3N_4 based catalysts. After potassium doping, an isolated atomic orbital of dopant may locate in the g-C_3N_4 band gap or orbital hybridization occurs between dopant orbital and molecular orbital of g-C_3N_4, leading to the altered potential of VB and CB.

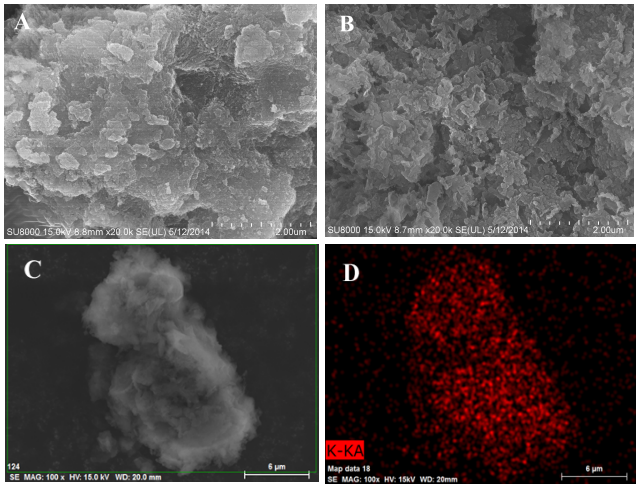

Fig. 4 SEM images of g-C_3N_4 (A), K(0.05)-CN (B, C) and elemental mapping image of K (D).

The morphologies of the representative samples were examined by using SEM analysis. Fig. 4C indicates as-prepared g-C_3N_4 based catalyst with a large number of irregular particles. Those particles exhibit layer structure that is similar to its analogue graphite (Fig. 4A and B). The size of layered structure of K(0.05)-CN is obviously decreased compared with g-C_3N_4. This indicates that potassium doping could inhibit crystal growth of graphitic carbon nitride, which is consistent with the XRD result. The elemental mapping image shown in Fig. 4D indicates that potassium is homogenously distributed in the whole host of g-C_3N_4. The potassium concentration obtained by ICP is 0.68,

1.35, 1.88, 2.3 and 1.39 wt.% in K(0.02)-CN, K(0.05)-CN, K(0.07)-CN, K(0.09)-CN and g-C_3N_4/KOH, respectively.

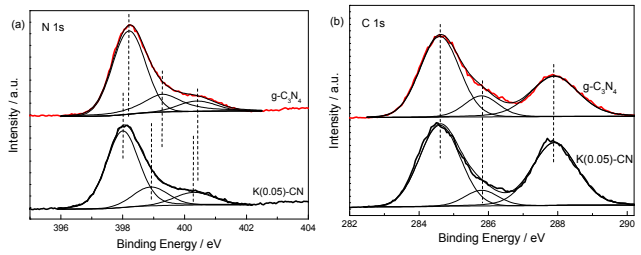

Fig. 5 XP spectra of as-prepared g-C_3N_4 based catalysts in the region of N 1s (a), C 1s (b), K 2p (c) and VB XPS (d).

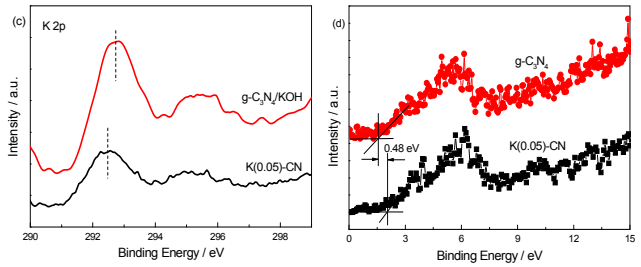

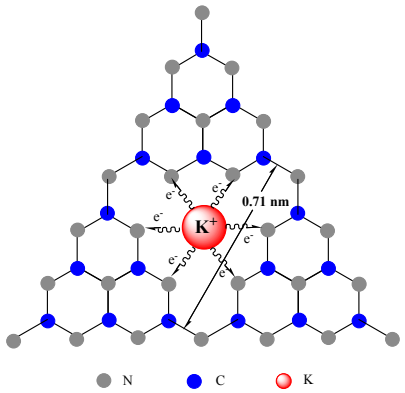

Fig. 6 The possible doping site of K ions in K(x)-CN.

XPS measurements were performed to explicate the valence states of various species. Fig. 5 displays the XP spectra of as-prepared g-C_3N_4 based catalysts in the region of N 1s (a), C 1s (b), K 2p (c) and VB XPS (d). In Fig. 5a and b, the spectra of g-C_3N_4 in both N 1s and C 1s regions can be fitted with three contributions. For N 1s region (Fig. 5a), three contributions located at 398.2, 399.3 and 400.4 eV are assigned to the sp^2 hybridized aromatic nitrogen atoms bonded to carbon atoms (C-N=C), tertiary nitrogen N-$(C)_3$ groups linking structural motif and nitrogen atoms bonded to three carbon atoms in the aromatic cycles.[26] In Fig. 5b, the component at 284.6 eV corresponds to C-C originates from pure graphitic carbon presumably formed during minor decomposition of the carbon nitride.[27] The peak at 285.8 eV corresponds to C=N or C≡N, which could be ascribed to defect containing sp^2-hybridized carbon atoms present in graphitic domains.[28] The peak at 287.9 eV corresponds to the sp^2-hybridized carbon in N=C-N_2 coordination, which connected with three neighboring N atoms in one double and two single bonds.[29] In the case of K(0.05)-CN, a slight shift to lower binding energy is observed in N 1s but not in C 1s region compared with that of g-C_3N_4. This is probably due to higher electronegativity of N atoms, leading to the formation of strong interaction with doped potassium. The electrons of potassium could be transferred to nitrogen, which caused the increasing electron density of N atoms.

Fig. 5c shows that the binding energy of g-C_3N_4/KOH in K 2p region is located at 292.7 and 295.5 eV, which should be attributed to the $2p_{3/2}$ and $2p_{1/2}$ in K-O group.[30,31] In the case of K(0.05)-CN, a obvious shift to lower binding energy (0.2 eV) is observed. Besides, the calculation result of surface elemental concentration determined by XPS reveals that K concentration in K(0.05)-CN is 1.46 wt.%, which is close to the ICP result (1.35 wt.%). In the case of g-C_3N_4/KOH, this value is 3.3 wt.%, much higher than that of ICP result (1.39 wt.%). This is probably due to the different existence form of K species in two samples. In the case of g-C_3N_4/KOH, K species mainly exists on the surface. Whereas K could be doped into g-C_3N_4 lattice in the formation of K-N bond during the polycondensation process, leading to the uniform dispersion in the bulk of K(0.05)-CN. Moreover, because the electronegativity of N atoms is lower than O atoms, the electron density of potassium in K-N bond should be higher than that in K-O group, leading to the binding energy difference (Fig. 5c). Besides, the XP spectra of K(0.05)-CN and g-C_3N_4/KOH in K 2s region are shown below (Fig. S5). The binding energy is located at 377.2 eV for K(0.05)-CN, which is in good agreement with the reported binding energy of K 2s for KN_3.[32] This indicates that the ions of K is coordinated into the big C-N rings formed by N-bridge linking the triazine units in the plane of g-C_3N_4. In the case of g-C_3N_4/KOH, no obvious peak is observed, which confirms our conclusion. It is known that the lone pair electron of nitrogen plays an important role in the electron density distribution, which has a strong influence on the electronic structure of carbon nitride.[33] K doping could change the electron density of N atoms, thus altered the electronic structure and band gap of carbon nitride. As for the doping site of potassium, the probably situation is interstitial site. The ionic radius of K is much larger than that of C and N, the substitutional doping should not occur. The maximum in-planar distance of nitride pores is 0.71 nm,[34] which is adequate to accommodate K ions. In addition, it is well known that the C-O ring in 18-crown-6 exhibits the strong capability to capture metal cations such as K^+ by forming an ion-dipole interaction between the cations and the negatively charged oxygen of the polyether ring.[35] Compared to the oxygen atoms in the C-O ring of 18-crown-6, the nitrogen atoms of the nitrogen pots of g-C_3N_4 are also ideal sites for metal ion inclusion with stronger coordination ability due to more lone-pair electrons. Summarizing the above results, the possible doping site of K ions in K(x)-CN is shown in Fig. 6.

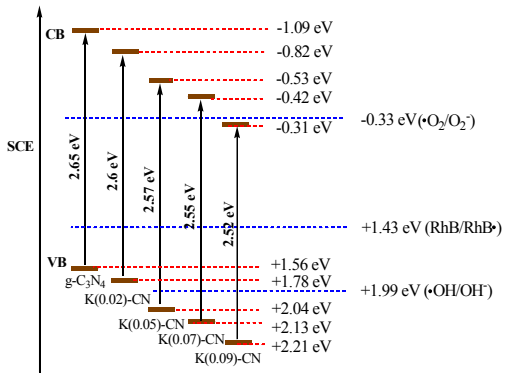

Fig. 7 Band gap structures of as-prepared g-C_3N_4 and K(x)-CN.

To further investigation the influence of K doping on the relative positions of the CB and VB, the VB XP spectra was employed to determine the electronic structure (Fig. 5d). Compared with the spectrum of g-C_3N_4, an obvious shift (0.48 eV) is shown in K(0.05)-CN, which could be attributed to the K doping. The VB potentials of g-C_3N_4 and K(0.05)-CN locate at +1.56 and +2.04 eV. Combined with the UV-Vis results, the optical CB potentials of g-C_3N_4 and K(0.05)-CN locate at -1.09 and -0.53 eV. The VB XP spectra of K(0.02)-CN, K(0.07)-CN and K(0.09)-CN are shown in Fig. S6. Their VB and CB potentials are also calculated and shown in Fig. 7. Obviously, the CB and VB positions obviously alters after K doping. The CB and VB potentials could be tuned from -1.09 and +1.56 eV to -0.31 and +2.21 eV by controlling the K concentration. Such tunable CB and VB potentials are beneficial to the forming of the heterojunction with other semiconductor in order to meet different application demands.

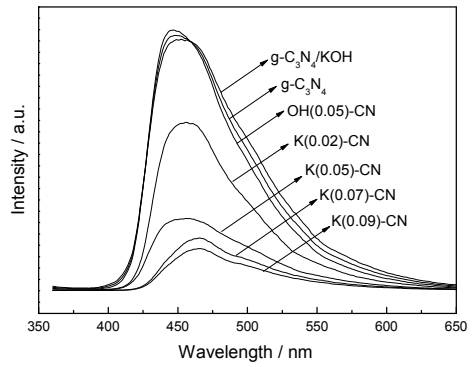

Fig. 8 PL spectra of as-prepared g-C_3N_4 based catalysts.

PL is a highly sensitive technique used to provide information on charge separation/recombination of photoinduced charged carriers.[36] In general, the lower PL intensity, the higher separation rate of photogenerated electron-hole pairs. Fig. 8 shows the PL spectra of as-prepared g-C_3N_4 based catalysts under the excitation wavelength of 380 nm at room temperature. For g-C_3N_4, the broad PL band is around 465 nm, which is attributed to the band-band PL phenomenon with the energy of light approximately equal to the band gap of g-C_3N_4.[37] Such band-band PL signal is attributed to excitonic PL, which mainly results from the n-π* electronic transitions involving lone pairs of nitrogen atoms in g-C_3N_4.[27] In the case of K(x)-CN, the shape of the curves are similar to that of g-C_3N_4, whereas the peak intensities decrease sharply. Such increased separation rate of photogenerated electrons-holes pairs in K(x)-CN catalysts could improve the visible light utilization, thus is beneficial to the photocatalytic performance. No essential difference in PL curves among g-C_3N_4/KOH, OH(0.05)-CN and K(0.05)-CN is observed, indicating those two modification methods did not improve the separation rate of photogenerated electrons-holes pairs. This result not only confirms the different existence form of K species between K(0.05)-CN and g-C_3N_4/KOH, but also suggests that such increased separation rate of electron-hole pairs for K(x)-CN is not caused by the alkalization treatment but by K doping. K doping gives rise to distortion in the lattice structure of g-C_3N_4. That caused the increased surface energy, leading to the reduced recombination rate of electron-hole pairs, enhancing the interfacial charge transfer rate.

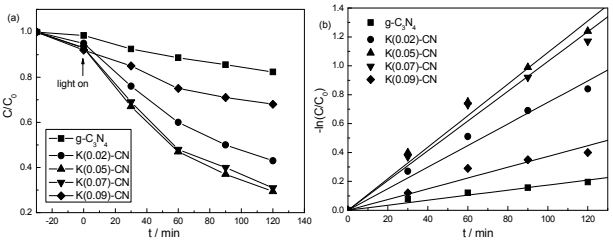

Fig. 9 Photocatalytic performances of as-prepared g-C_3N_4 based catalysts (a) and plot of -ln(C/C_0) against reaction time (b) in the degradation of RhB under visible light irradiation.

Fig. 9a shows the photocatalytic performances of as-prepared g-C_3N_4 based catalysts in the degradation of RhB under visible light irradiation. Before the light on, the RhB adsorption abilities of K(x)-CN catalysts are enhanced, which is probably due to the larger S_{BET}. Control experiment results indicate that the RhB degradation performance could be ignored in the absence of either irradiation or photocatalyst, indicating that RhB is degraded via photocatalytic process. Fig. S7 shows that g-C_3N_4/KOH and OH(0.05)-CN exhibit almost the same photocatalytic activity as g-C_3N_4. Whereas K(x)-CN catalysts show clearly higher activities than that of g-C_3N_4 (Fig. 9a). This is probably due to the synergistic effect caused by the K doping which improved the S_{BET}, decreased the band gap energy and enhanced the separation rate of photogenerated electron-hole pairs. The photocatalytic activity enhances gradually with increasing the K concentration from 0.02 to 0.05. K(0.05)-CN and K(0.07)-CN show much higher photocatalytic activity than that of other potassium doped catalysts. When the K concentration beyond 0.07, the activity decrease remarkably. The possible reason is discussed (see below). The reaction rate constant k is obtained by assuming that the reaction followed first order kinetics.[38] Fig. 9b displays that a linear relationship is established when -ln(C/C_0) is plotted against t (reaction time). The rate constant k can be calculated by the slope of the curve. The results indicate that the rate constant k are 0.0017, 0.0074,

0.011, 0.010 and 0.0037 min^{-1} for g-C_3N_4, K(0.02)-CN, K(0.05)-CN, K(0.07)-CN and K(0.09)-CN, respectively. K(0.05)-CN shows the highest rate constant, which is 6.4 times higher than that of g-C_3N_4.

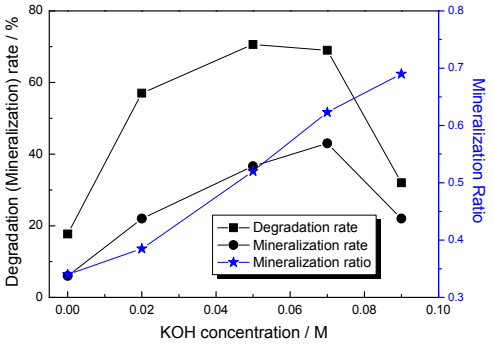

Fig. 10 Degradation rate, mineralization rate and mineralization ratio comparison of as-prepared g-C_3N_4 based catalysts.

The mineralization ability of prepared catalysts to RhB molecules was evaluated by monitoring the changes of TOC in the reaction systems. Fig. 10 shows the degradation rate, mineralization rate and mineralization ratio comparison of as-prepared g-C_3N_4 based catalysts. Mineralization ratio, which represents the mineralization ability is equal to the ratio of the mineralization rate to the degradation rate. Obviously, the mineralization rates of as-prepared g-C_3N_4 based catalysts show a similar variation trend to the degradation rate. However, the mineralization ratio increases evidently with increasing the KOH concentration. Zhang et al. prepared TCNQ-g-C_3N_4 organic composite photocatalysts for phenol degradation. They suggested that the enhancement of mineralization ability was attributed to the lower valence position which caused by the formation of conjugative π structure material hybridized photocatalysts.[39] In this investigation, potassium doping can alter the band structure of as-prepared g-C_3N_4 based catalysts, thus improve the mineralization ability.

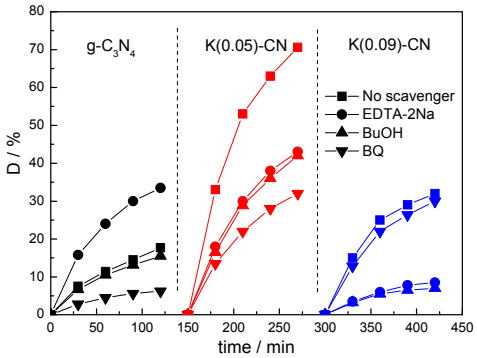

Fig. 11 Influence of various scavengers on the visible light photocatalytic activity of g-C_3N_4, K(0.05)-CN and K(0.09)-CN.

The catalytic stability test of as-prepared K(0.05)-CN was carried out (Fig. S8). The results indicate that no obvious decrease in RhB degradation performance is observed after three cycles. The XPS curves of fresh and reused K(0.05)-CN reveal that the chemical state of potassium element is not changed (Fig. S9). Moreover, ICP result displays that the potassium concentration is 1.33 wt.% in reused K(0.05)-CN which is very close to the fresh catalyst (1.35 wt.%). Therefore, it is deduced that the as-prepared K(0.05)-CN is stable. However, the ICP result indicates that the potassium concentration of used g-C_3N_4/KOH decreases sharply to 0.44 wt.%, probably due to that KOH dissolved into the solution. To confirm this point, the pH values of K(0.05)-CN and g-C_3N_4/KOH suspension were measured by a pH meter. The results show that the suspension of K(0.05)-CN is almost neutral (pH=7.17). In the case of g-C_3N_4/KOH, the pH value is 9.25, much higher than that of K(0.05)-CN.

The hole and free radical trapping experiments were carried out to clarify the reaction mechanism and the active species generated during the reaction process. In this investigation, EDTA-2Na, tert-butyl alcohol (t-BuOH) and 1,4-benzoquinone (BQ) are used as the hole (h^+), hydroxyl radical (•OH) and superoxide radical ($•O_2^-$) scavenger, respectively.[40] Fig. 11 shows the influence of various scavengers on the visible light photocatalytic activity of g-C_3N_4, K(0.05)-CN and K(0.09)-CN. For g-C_3N_4, the photodegradation rate of RhB only decreases slightly after the addition of t-BuOH, but sharply when BQ is added. This indicates that the main active species is not hydroxyl radicals but $•O_2^-$ in the current photocatalytic systems. In theory, the CB and VB position of g-C_3N_4 are -1.12 V and +1.57 V, respectively.[41] The redox potentials of $•OH/OH^-$ and $O_2/•O_2^-$ are +1.99 V and -0.33 V, as shown in Fig. 7.[42] Obviously, the reduction potential of CB electrons in g-C_3N_4 is more negative than the redox potential of $O_2/•O_2^-$ which can reduce O_2 to form $•O_2^-$, whereas the VB holes in g-C_3N_4 are not positive enough to generate •OH. This theoretical result is consistent with our experiment results. In the presence of EDTA-2Na, the degradation rate is increased obviously, which is completely different from previous results.[38] Zhang et al. prepared $C_3N_4/Bi_5Nb_3O_{15}$ heterojunction catalyst for 4-CP photodegradation.[40] The photodegradation rate decreased significantly after the addition of EDTA-2Na, indicating the photogenerated holes were the main active species in their system. In this study, although the redox potential of RhB is reported to be 1.43 V,[43] which is higher than the VB of g-C_3N_4 (Fig. 7), the direct photogenerated holes oxidation did not occur. On the contrary, the addition of EDTA-2Na to trap the h^+ could promote the separation rate of electron-hole pairs, leading to the increased photocatalytic performance. In the case of K(0.05)-CN, the activity decreases obviously when each scavenger is added, suggesting both •OH and $•O_2^-$ are the main active species in this photocatalytic system. This is due to the change of VB and CB positions after potassium doping. The VB potential is +2.04 eV, more positive than the redox potential of $•OH/OH^-$. Therefore, OH^- could trap the h^+ to form •OH, which is responsible for RhB degradation. For K(0.09)-CN, the VB and CB potentials are +2.21 and -0.31 eV, as shown in Fig. 7. The CB potential decreases obviously, even lower than that of redox potential of $O_2/•O_2^-$. Therefore, when BQ is added, only slight decrease in activity is observed. Moreover, the addition of EDTA-2Na and BuOH remarkably decrease the activity confirms that the main active species is •OH in this photocatalytic system. Because the

positions of VB and CB of K(x)-CN are obviously altered after potassium doping, both •OH and $•O_2^-$ could be formed in K(0.05)-CN and K(0.07)-CN systems (Fig. 7). Therefore, it is reasonable that K(0.05)-CN and K(0.07)-CN show much higher activities than that of other potassium doped catalysts.

To further prove the effectiveness of alkali metal modification, we used this approach to synthesize sodium doped g-C_3N_4 catalysts. The preparation method is same as that of K(x)-CN but using NaOH instead of KOH. Fig. S10 indicates that the photocatalytic activities increase obviously after sodium doping. From the color of as-prepared sodium doped g-C_3N_4 catalysts, the band structure could also be altered by sodium doping. These results prove that alkali metal modification is a facile and flexible approach for the synthesis of carbon nitride photocatalyst with a tunable band structure. Such tunable band structure of g-C_3N_4 is beneficial for the forming of heterojunction with other semiconductor for different application demands.

Conclusions

A novel alkali metal potassium doped carbon nitride photocatalyst with a tunable band structure was prepared using dicyandiamide monomer and potassium hydrate as precursor. Potassium doped g-C_3N_4 exhibited smaller grain size, larger S_{BET}, narrower band gap energy and better separation rate of photogenerated electrons and holes. The contrast experiment results indicated that those changes are not caused by the alkalization treatment but by potassium doping. The CB and VB potentials of as-prepared K(x)-CN were obviously altered by increasing the potassium concentration. The RhB photodegradation and mineralization abilities under visible light were significantly improved after potassium doping. Because of the regulating effect of potassium doping on band structure, both •OH and $•O_2^-$ could be formed in K(0.05)-CN and K(0.07)-CN system, leading to their activities much higher than that of other potassium doped catalysts. K(0.05)-CN shows the highest rate constant, which is 6.4 times higher than that of g-C_3N_4. Moreover, K(0.05)-CN exhibited stable catalytic activity and chemical structure. Sodium doped g-C_3N_4 catalysts prepared by the similar method also exhibited the tunable band structure and improved photocatalytic performance.

Acknowledgment

This work was supported by National Natural Science Foundation of China (No. 41071317, 30972418), National Key Technology R & D Programme of China (No. 2007BAC16B07, 2012ZX07505-001), the Natural Science Foundation of Liaoning Province (No. 20092080), Education Department of Liaoning Province (No. L2014145) and the Natural Science Foundation of Liaoning Shihua University (No. 2011XJJ-021).

Notes and references

[a] *Institute of Eco-environmental Sciences, Liaoning Shihua University, Fushun 113001, PR China. E-mail: hushaozhenglnpu@163.com; Tel: 86-24-56860865*

[b] *School of Environmental and Biological Engineering, Liaoning Shihua University, Fushun 113001, PR China*

[c] *School of Petrochemical Engineering, Liaoning Shihua University, Fushun 113001, PR China. E-mail: lvzhenbolnpu@163.com*

1 J.S. Zhang, G.G. Zhang, X.F. Chen, S. Lin, L. Möhlmann, G. Lipner, M. Antonietti, S. Blechert and X.C. Wang, *Angew. Chem. Int. Ed.*, 2012, **51**, 3183.
2 Y.Y. Bu, Z.Y. Chen and W.B. Li, *Appl. Catal. B: Environ.*, 2014, **144**, 622.
3 J. Xu, H.T. Wu, X. Wang, B. Xue, Y.X. Li and Y. Cao, *Phys. Chem. Chem. Phys.*, 2013, **15**, 4510.
4 K. Sridharan, E. Jang and T.J. Park, *Appl. Catal. B: Environ.*, 2013, **142-143**, 718.
5 P. Niu, L. Zhang, G. Liu and H. Cheng, *Adv. Funct. Mater.*, 2012, **22**, 4763.
6 D.C. Pan, D. Weng, X.L. Wang, Q.F. Xiao, W. Chen, C.L. Xu, Z.Z. Yang and Y.F. Lu, *Chem. Commun.*, 2009, **28**, 4221.
7 S.Z. Hu, R.R. Jin, G. Lu, D. Liu and J.Z. Gui, *RSC Adv.*, 2014, **4**, 24863.
8 S.C. Yan, Z.S. Li and Z.G. Zou, *Langmuir*, 2010, **26**, 3894.
9 G. Liu, P. Niu, C.H. Sun, S.C. Smith, Z.G. Chen, G.Q. Lu and H.M. Cheng, *J. Am. Chem. Soc.*, 2010, **132**, 11642.
10 Y.J. Zhang, T. Mori, J.H. Ye and M. Antonietti, *J. Am. Chem. Soc.*, 2010, **132**, 6294.
11 L.G. Zhang, X.F. Chen, J. Guan, Y.J. Jiang, T.G. Hou and X.D. Mu, *Mater. Res. Bull.*, 2013, **48**, 3485.
12 G.G. Zhang, M.W. Zhang, X.X. Ye, X.Q. Qiu, S. Lin and X.C. Wang, *Adv. Mater.*, 2014, **26**, 805.
13 S.Z. Hu, L. Ma, J.G. You, F.Y. Li, Z.P. Fan, G. Lu, D. Liu and J.Z. Gui, *Appl. Surf. Sci.*, 2014, **311**, 164.
14 D. Salinas, P. Araya and S. Guerrero, *Appl. Catal. B: Environ.*, 2012, **117-118**, 260.
15 H. Chu, L.J. Yang, Q.H. Zhang and Y. Wang, *J. Catal.*, 2006, **241**, 225.
16 G. Pekridis, N. Kaklidis, M. Konsolakis, C. Athanasiou, I.V. Yentekakis and G.E. Marnellos, *Solid State Ionics*, 2011, **192**, 653.
17 Z.P. Qu, Y.B. Bu, Y. Qin, Y. Wang and Q. *Fu, Chem. Eng. J.*, 2012, **209**, 163.
18 J. Grzechulska, M. Hamerski and A.W. Morawski, *Water Res.*, 2000, **34**, 1638.
19 L.C. Chen, .M. Huang and F.R. Tsai, *J. Mol. Catal. A: Chem.*, 2007, **265**, 133.
20 F.B. Li, X.Z. Li, M.F. Hou, K.W. Cheah and W.C.H. Choy, *Appl. Catal. A: Gen.*, 2005, **285**, 181.
21 Y. Wang, X.C. Wang and M. Antonietti, *Angew. Chem. Int. Ed.*, 2012, **51**, 68.
22 S.C. Yan, Z.S. Li and Z.G. Zou, *Langmuir*, 2009, **25**, 10397.
23 L. Liu, D. Ma, H. Zheng, X.J. Li, M.J. Cheng and X.H. Bao, *Micro. Meso. Mater.*, 2008, **110**, 216.
24 Y.I. Kim, S.J. Atherton, E.S. Brigham and T.E. Mallouk, *J. Phys. Chem.,* **1993**, *97*(45), 11802.
25 G.Q. Li, N. Yang, W.L. Wang and W.F. Zhang, *J. Phys. Chem. C*, 2009, **113**, 14829.
34 X.G. Ma, Y.H. Lv, J. Xu, Y.F. Liu, R.Q. Zhang and Y.F. Zhu, *J. Phys. Chem. C*, 2012, **116**, 23485.
26 Y.W. Zhang, J.H. Liu, G. Wu and W. Chen, *Nanoscale*, 2012, **4**, 5300.
27 V.N. Khabashesku, J.L. Zimmerman and J.L. Margrave, *Chem. Mater.*, 2000, **12**, 3264.
28 W. Lei, D. Portehault, R. Dimova and M. Antoniettit, *J. Am. Chem. Soc.*, 2011, **133**, 7121.
29 Q.X. Guo, Y. Xie, X.J. Wang, S.Y. Zhang, T. Hou and S.C. Lv, *Chem. Commun.*, 2004, 26.
30 A. Miyakoshi, A. Ueno and M. Ichikawa, *Appl. Catal. A: Gen.*, 2001, **219**, 249.
31 M. Muhler, R. Schlogl and G. Ertl, *J. Catal.*, 1992, **138**, 413.
32 J. Sharma, T. Gora, J.D. Rimstidt and R. Staley, *Chem. Phys. Lett.,* 1972, **15**, 232.
33 G.P. Dong, Y.H. Zhang, Q.W. Pan and J.R. Qiu, *J. Photochem. Photobiol. C: Photochem. Rev.*, 2014, **20**, 33.
35 C. J. Pedersen, *J. Am. Chem. Soc.*, 1967, **89**, 7017.
36 H. Nakajima, T. Mori, Q. Shen and T. Toyoda, *Chem. Phys. Lett.*, 2005, **409**, 81.
37 L. Ge and C. Han, *Appl. Catal. B: Environ.*, 2012, **117-118**, 268.

38 X.Y. Li, D.S. Wang, G.X. Cheng, Q.Z. Luo, J. An and Y.H. Wang, *Appl. Catal. B: Environ.*, 2008, **81**, 267.
39 M. Zhang, W.Q. Yao, Y.H. Lv, X.J. Bai, Y.F. Liu, W.J. Jiang and Y.F. Zhu, *J. Mater. Chem. A*, 2014, **2**, 11432.
40 S.Q. Zhang, Y.X. Yang, Y.N. Guo, W. Guo, M. Wang, Y.H. Guo and M.X. Huo, *J. Hazard. Mater.*, 2013, **261**, 235.
41 X.C. Wang, K. Maeda, A. Thomas, K. Takanabe, G. Xin, K. Domen and M. Antonietti, *Nat. Mater.*, 2009, **8**, 76.
42 G. Liu, P. Niu, L.C. Yin and H.M. *J. Am. Chem. Soc.*, 2012, **134**, 9070.
43 T. Shen, Z.G. Zhao, Q. Yu and H.J. Xu, *J. Photochem. Photobiol. A: Chem.*, 1989, **47**, 203.